Photocatalytic inactivation of viruses using graphitic carbon nitride-based photocatalysts

Hasija, Vasudha; Patial, Shilpa; Singh, Pardeep; Nguyen, Van Huy; Van Le, Quyet; Thakur, Vijay Kumar; Hussain, Chaudhery Mustansar; Selvasembian, Rangabhashiyam; Huang, Chao Wei; Thakur, Sourbh; Raizada, Pankaj

Published in:
Catalysts

DOI:
10.3390/catal11121448

First published: 28/11/2021

Document Version
Publisher's PDF, also known as Version of record

catalysts

MDPI

Review

Photocatalytic Inactivation of Viruses Using Graphitic Carbon Nitride-Based Photocatalysts: Virucidal Performance and Mechanism

Vasudha Hasija [1], Shilpa Patial [1], Pardeep Singh [1], Van-Huy Nguyen [2], Quyet Van Le [3], Vijay Kumar Thakur [4,5], Chaudhery Mustansar Hussain [6], Rangabhashiyam Selvasembian [7], Chao-Wei Huang [8,*], Sourbh Thakur [9] and Pankaj Raizada [1,*]

1 School of Advanced Chemical Sciences, Shoolini University, Solan 173229, Himachal Pradesh, India; vasudhahasija10@gmail.com (V.H.); shilpapatial26@gmail.com (S.P.); pardeepchem@gmail.com (P.S.)
2 Faculty of Biotechnology, Binh Duong University, Thu Dau Mot 820000, Vietnam; nvhuy@bdu.edu.vn
3 Department of Materials Science and Engineering, Korea University, 145 Anam-ro Seongbuk-gu, Seoul 02841, Korea; quyetbk88@korea.ac.kr
4 Biorefining and Advanced Materials Research Centre, SRUC, Edinburgh EH9 3JG, UK; vijay.thakur@sruc.ac.uk
5 School of Engineering, University of Petroleum & Energy Studies (UPES), Dehradun 248001, Uttarakhand, India
6 Department of Chemistry and Environmental Science, New Jersey Institute of Technology, Newark, NJ 07102, USA; chaudhery.m.hussain@njit.edu
7 Department of Biotechnology, School of Chemical and Biotechnology, SASTRA Deemed University, Thanjavur 613401, Tamil Nadu, India; rambhashiyam@gmail.com
8 Department of Chemical and Materials Engineering, National Kaohsiung University of Science and Technology, Kaohsiung 80778, Taiwan
9 Department of Organic Chemistry, Bioorganic Chemistry and Biotechnology, Silesian University of Technology, B. Krzywoustego 4, 44-100 Gliwice, Poland; Sourbh.Thakur@polsl.pl
* Correspondence: huangcw@nkust.edu.tw (C.-W.H.); pankajchem1@gmail.com (P.R.)

Abstract: The prevalence of lethal viral infections necessitates the innovation of novel disinfection techniques for contaminated surfaces, air, and wastewater as significant transmission media of disease. The instigated research has led to the development of photocatalysis as an effective renewable solar-driven technology relying on the reactive oxidative species, mainly hydroxyl ($OH^{\bullet}$) and superoxide ($O_2^{\bullet-}$) radicals, for rupturing the capsid shell of the virus and loss of pathogenicity. Metal-free graphitic carbon nitride (g-C_3N_4), which possesses a visible light active bandgap structure, low toxicity, and high thermal stability, has recently attracted attention for viral inactivation. In addition, g-C_3N_4-based photocatalysts have also experienced a renaissance in many domains, including environment, energy conversion, and biomedical applications. Herein, we discuss the three aspects of the antiviral mechanism, intending to highlight the advantages of photocatalysis over traditional viral disinfection techniques. The sole agenda of the review is to summarize the significant research on g-C_3N_4-based photocatalysts for viral inactivation by reactive oxidative species generation. An evaluation of the photocatalysis operational parameters affecting viral inactivation kinetics is presented. An overview of the prevailing challenges and sustainable solutions is presented to fill in the existing knowledge gaps. Given the merits of graphitic carbon nitride and the heterogeneous photocatalytic viral inactivation mechanism, we hope that further research will contribute to preventing the ongoing Coronavirus pandemic and future calamities.

Keywords: viral inactivation; photocatalysis; graphitic carbon nitride; healthcare

check for updates

Citation: Hasija, V.; Patial, S.; Singh, P.; Nguyen, V.-H.; Le, Q.V.; Thakur, V.K.; Hussain, C.M.; Selvasembian, R.; Huang, C.-W.; Thakur, S.; et al. Photocatalytic Inactivation of Viruses Using Graphitic Carbon Nitride-Based Photocatalysts: Virucidal Performance and Mechanism. *Catalysts* **2021**, *11*, 1448. https://doi.org/10.3390/catal11121448

Academic Editor: Magdalena Janus

Received: 21 October 2021
Accepted: 25 November 2021
Published: 28 November 2021

Publisher's Note: MDPI stays neutral with regard to jurisdictional claims in published maps and institutional affiliations.

1. Introduction

The outbreak of the Coronavirus infectious disease has drenched the world in devastating health impacts [1]. Globally, the Coronavirus pandemic has caused over 4 million

fatalities as of 28 July 2021 at a steady rate [2–4]. Hence, a paradigm approach to preparedness and a timely communal response are required to battle against the high contagiousness of viruses.

An emerging treatment strategy against viral outbreaks is the nanotechnology route of designing antiviral therapeutics [5]. Nano-antimicrobials (i.e., nanoparticle-derived antiviral agents) are of nanometer size, which makes them well-suited for biochemical interactions with a nanosized virus. The properties of nanoparticles behind the antiviral activity include the small size with a large surface area and the selective, targeted, and stimulus-responsive action on the virus [6]. The functionalization of carbon-based nanomaterials, including carbon quantum dots, graphene, graphene oxide, fullerenes, and graphitic carbon nitride, has been used in antiviral research under visible light irradiation for human immunodeficiency virus (HIV), avian influenza virus A (H1N1), poliovirus, herpes simplex virus, and human adenovirus [7].

Thereby, rigorous research is required to develop a facile, stable, cost-effective, highly efficient, and sustainable technique for disinfecting virus-contaminated water, air, and surfaces. Fortunately, an advanced oxidation process is a promising technology to alleviate infectious viruses in the environment. AOPs include ozonation, the homogenous photo-Fenton process, photo-electro-oxidation, ultrasound, and photocatalysis and can be used to efficiently treat virus contamination [8,9]. Certainly, photocatalysis is an advanced "green disinfection" strategy that targets wide-scale viruses present on surfaces and in air and wastewater owing to the high redox abilities of the produced reactive oxidative species (ROSs), such as hydroxyl ($OH^{\bullet}$), superoxide ($O_2^{\bullet -}$), hole (h^+), and peroxide (O_2^{-2}) radicals [10,11]. A broad survey of literature on photocatalytic systems for virus disinfection is presented in Table 1 [12–31], further instigating researchers to exploit photocatalysis against SARS-CoV-2.

Table 1. Summary of potential photocatalysts for virus disinfection.

Photocatalyst	Virus	Light Source	Wavelength	Virus Level	Major Reactive Species	Inactivation Efficiency/Time	Ref.
Ag doped TiO_2	Hepatitis B	UV cut-off filter	420 nm	1g/L	$OH^{\bullet}$, $O_2^{\bullet -}$	81.7 %/12 h	[12]
TiO_2 coated ceramic	Hepatitis B	Hg lamp (125 W)	365 nm	-	$OH^{\bullet}$, $HOO^{\bullet}$	97 % /240 min	[13]
TiO_2	Human adenovirus 40	UV lamp	254 nm	1×10^8 PFU/mL	$OH^{\bullet}$	0.49 log/14.3 min	[14]
TiO_2	Herpes simplex virus	UV-A lamp (Philips TLD 15 W/05)	365 nm	10^9–10^{10} PFU/mL	$OH^{\bullet}$, $O_2^{\bullet -}$	100 %/360 min	[15]
TiO_2	Influenza virus H9N2	UV (Black light 20W)	365 nm	1×10^4 PFU/mL	$OH^{\bullet}$	4-log/150 min	[16]
TiO_2	Influenza virus H1N1	UV-A light (Tubular 20 W black light fluorescent lamps)	352 nm	1×10^8 PFU/mL	$OH^{\bullet}$, $O_2^{\bullet -}$	5.2-log/480 min	[17]
TiO_2	Murine Norovirus	UV lamp (8 W)	385 nm	7.8 PFU/mL	$OH^{\bullet}$	4 log/10 min	[18]
Cu-doped TiO_2	Norovirus	UVA-LED	373 nm	2.89 ± 0.11 $\log_{10}$	$OH^{\bullet}$, $O_2^{\bullet -}$	5 log/60 min	[19]
TiO_2	Bacteriophage MS2, Murine Norovirus, Influenza	UV light Blacklight Blue lamps (BLB,4 W, Philips Co.	360 nm	1×10^6 PFU/mL	$OH^{\bullet}$	1.5×10^{-5} mg/L/36 min, 1.4×10^{-5} mg/L /32 min, 1.7×10^{-5} mg/L/40 min	[20]
ZnO	Bacteriophage MS2, ΦX174, PR772	UV-B	295 nm	1×10^5 PFU/mL	$OH^{\bullet}$	0.37, 0.67, 0.59 L/kJ/360 min	[21]
Ag-AgI/Al_2O_3	Human rotavirus type-II Wa	350-W Xe-arc lamp	450 nm	3.2×10^3 PFU/mL	$O_2^{\bullet -}$, h^+	3.2 log/40 min	[22]
Pt/WO_3 films	Influenza virus H1N1	Fluorescentlamps (FL20SS W/18) 1000 lx	470 nm	1×10^7 PFU/mL	$OH^{\bullet}$	>5.5 log/120 min	[23]
C_{60}	Rhabdoviridae	Hg lamp (350 W)	495 nm	10 log $TCID_{50}$/mL	$^1O_2$	7 log10 /360 min	[24]
C_{60}/SiO_2	Bacteriophage MS2	Fluorescent bulbs	470 nm	5×10^4 PFU/mL	$^1O_2$	3.55 log/75 min	[25]
C_{70}/SiO_2	Bacteriophage MS2	Visible, Sunlight	420 nm	3×10^8 PFU/mL	$^1O_2$	4.35 log; 4.4 log/90 min	[26]
g-C_3N_4	Bacteriophage MS2	Xenon lamp	400 nm	1×10^8 PFU/mL	$O_2^{\bullet -}$	6.58 log/180 min	[27]
g-C_3N_4	Bacteriophage MS2	300 W Xenon lamp	450 nm	1×10^8 PFU/mL	$O_2^{\bullet -}$	8 log/360 min	[28]
Ag_3PO_4/g-C_3N_4	Bacteriophage f2	UVA lamp (8W)	500 nm	3×10^7 PFU/mL	h^+	6.5 log/80 min	[29]
g-C_3N_4/Expanded perlite	Bacteriophage MS2	Xenon lamp (300 W)	300 nm	1×10^8 PFU/mL	$OH^{\bullet}$, $O_2^{\bullet -}$	8 log/240 min	[30]
O-doped g-C_3N_4	Human adenovirus	7 W LED lamp	450 nm	-	$OH^{\bullet}$, $O_2^{\bullet -}$, H_2O_2	5 log/120 min	[31]

In addition to metal-based semiconductors, carbon-based photocatalysts are potential candidates in this regard. Among all the antiviral photocatalysts, graphitic carbon nitride (g-C_3N_4)-based photocatalysts have emerged recently. With an analogous structure to graphene, g-C_3N_4 has a unique hexagonal framework with C-N bonds in place of C-C bonds and is a sustainable alternative to metal-based materials [32]. The exceptional properties of g-C_3N_4 include exceptionally high thermal stability, versatile physicochemical, optical, and electronic properties, and a wide range of synthesis routes, which promote its application in heterogeneous catalysis, environmental remediation, the conversion of energy into usable fuels, and the biomedical field [33]. Several comprehensive reviews have systematically summarized the synthesis, properties, and applications of g-C_3N_4 photocatalysts [34–36]. Additionally, there are reviews on the use of metal oxides [37], graphene [38], and carbon-based nanomaterials [39] for controlling the SARS-CoV-2 virus. This review seeks to provide a complete overview of the g-C_3N_4-based photocatalysts applied for virus disinfection in wastewater. The aim of the review is to make readers understand the potential of photocatalysis phenomena in relevance to virus disinfection. The following section provides an overview of the antiviral performance of g-C_3N_4-based photocatalysts by discussing the relevant reported research. Furthermore, innovative research in the healthcare realm, including pathogenic biofilm control, therapeutics, and bioimaging, using graphitic carbon nitride-based photocatalysts is reviewed. Finally, challenges and possible sustainable solutions for designing g-C_3N_4-based photocatalysts for viral inactivation purposes during the pandemic and beyond are addressed.

2. Photocatalytic Virus Inactivation: Mechanism

The use of photocatalysis technology in virus inactivation was first reported over a TiO_2 photocatalyst for MS2 phage inactivation by destroying the protein capsids upon the oxidative action of $OH^{\bullet}$ radicals [40]. Since then, the development of photocatalytic antiviral agents has been ever-increasing, with a paradigm shift in research from metal-oxide-based photocatalysts to metal-free visible light active photocatalysts [41]. It is worth clarifying that the photocatalytic viral inactivation process targets the structure of the virus, involving genetic core (RNA or DNA) damage, protein oxidation, and shape rupturing/distortion. Viral inactivation by the photocatalysis process is proposed [42] to occur by three routes, as shown in Figure 1, which are: (i) physical damage to capsid protein shells of viruses that causes their inactivation; (ii) metal ion toxicity in synergism with photocatalysis that induces the release of metal ions to increase the speed of viral inactivation kinetics; and (iii) chemical oxidation, which is the most effective photocatalytic virus disinfection process due to the participation of reactive oxidative species with strong oxidizing power that target the degradation of the cell wall and cytoplasmic membrane of the virus.

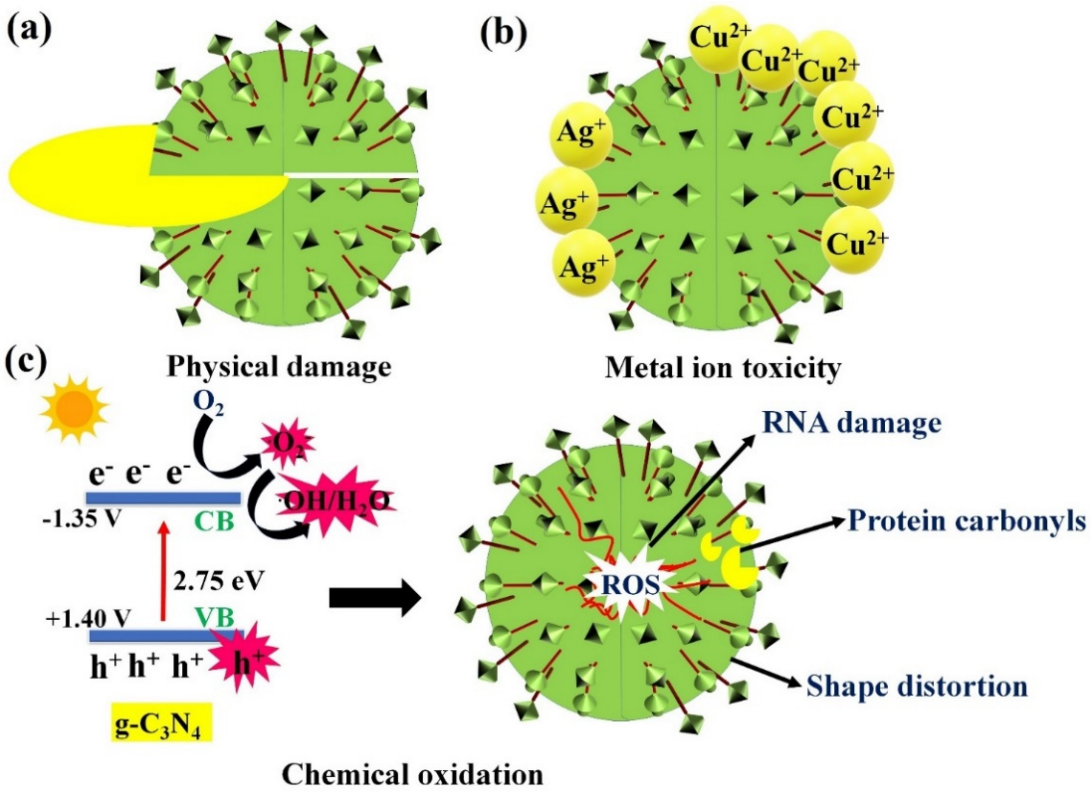

Figure 1. Proposed mechanisms of viral inactivation induced by photocatalysts via different routes (**a**) physical damage induced by rupturing of cell wall, (**b**) attack of metal ions, and (**c**) action of reactive oxidation species (ROS). Reproduced with permission from [42] with license number 5191840171112. Copyright Elsevier 2019.

In brief, photocatalytic viral inactivation utilizes renewable solar energy and an abundance of oxygen to generate reactive oxidative species. The photocatalytic virus inactivation has the following step-wise mechanism: (i) upon irradiation with light, semiconductor-based photocatalysts induce the production of electron–hole pairs with the simultaneous migration of charges to the reactive surface; (ii) the holes in the valence band react with the H_2O molecules or surface-adsorbed OH species to produce $OH^{\bullet}$, which targets the chemical composition of the shells and capsids of viruses; and (iii) the electrons in the conduction band react with the molecular oxygen (O_2) for the production of highly reactive radicals, including $O_2^{\bullet -}$, $OH^{\bullet}$, and O_2^{-2}, which attack the virus adsorbed on the photocatalytic surface [43,44]. Figure 1c illustrates the sequential heterogenous photocatalytic viral inactivation mechanism, wherein the released reactive species oxidize viruses by damaging coenzyme A on the cell membrane, causing inhibition of cellular respiration activity and eventual cell death [45,46]. The mechanistic action of ROSs for enveloped viruses (influenza, Hepatitis B [13], Rhabdoviridae [24], etc.) follows a different route of inactivation due to the assembly of the structural proteins (i.e., the spike, nucleocapsid, membrane, and envelope proteins). The plausible attack of ROS on enveloped viruses, as summarized by Costa et al. [47], includes: (i) alteration of protein cross-linkage; (ii) destruction of the protein structure; and (iii) variation in the charge and mass. For instance, Korneev et al. [48] investigated the photodynamic inactivation performance of the photosensitizer octacationic octakis(cholinyl) zinc phthalocyanine on influenza virus and observed an attack of singlet oxygen on spike glycoproteins. The TEM images indicated baldness of virions at higher concentrations of photosensitizer (4 μM) upon light exposure for more prolonged durations, leading to baldness of the virion and its infectivity. Regarding photocatalysis, as an alternative route for combatting enveloped SARS-CoV-2, an understanding of the actual mechanism of virus inactivation is vital. To date, diverse photocatalysts have been explored for photocatalytic viral inactivation; however, the research has yet to yield large scale application.

3. Antiviral Characteristics of Graphitic Carbon Nitride

Graphitic carbon nitride (g-C_3N_4) is emerging in the field of antiviral photoactivity mainly due to its metal-free composition, non-toxic nature, biocompatibility, photocorrosion resistance, and chemically stable features [49]. The facile fabrication of g-C_3N_4 by nitrogen-rich organic precursors (e.g., urea, melamine, thiourea, cyanamide, and dicyanamide) enables low-cost and bulk fabrication [50]. Bulk g-C_3N_4 possesses a suitable bandgap of 2.7 eV, promoting visible light absorption up to 460 nm. According to the bandgap structure of g-C_3N_4, the valence band potential (+1.4 eV vs. NHE) is thermodynamically unfavorable for the production of $OH^\bullet$ ($H_2O/OH^\bullet$ = 2.38 eV vs. NHE; $OH^-/OH^\bullet$ = +1.99 eV vs. NHE) [51]. Hence, many reports claim that viral inactivation in the g-C_3N_4 disinfection system is due to the photogenerated-h^+-dominant oxidation process [52,53]. Benefitting from the appropriate positioning of the conduction band (−1.1 eV vs. NHE), the facile production of $O_2^{\bullet-}$ occurs by favorably reducing O_2 into $O_2^{\bullet-}$ ($O_2/O_2^{\bullet-}$ = −0.33 eV vs. NHE). The subsequent formation of $OH^\bullet$ via multistep reduction of O_2 at the reductive site of g-C_3N_4 was identified in MS2 bacteriophage inactivation [27]. Overall, the photocatalytic electron transfer and ROS generation are described by Equations (1)–(7) [54].

$$g - C_3N_4 + h\nu \rightarrow g - C_3N_4\left(e^-_{CB} + h^+_{VB}\right) \quad (1)$$

$$g - C_3N_4\left(h^+_{VB}\right) + H_2O \rightarrow g - C_3N_4 + OH^\bullet + h^+ \quad (2)$$

$$g - C_3N_4\left(h^+_{VB}\right) + OH^- \rightarrow g - C_3N_4 + OH^\bullet \quad (3)$$

$$g - C_3N_4\left(e^-_{CB}\right) + O_2 \rightarrow g - C_3N_4 + O_2^{\bullet-} \quad (4)$$

$$O_2^{\bullet-} + HO_2^\bullet + H^+ \rightarrow OH^\bullet + O_2 + H_2O_2 \quad (5)$$

$$2HO_2^{\bullet-} + 2H^+ \rightarrow O_2 + H_2O_2 \quad (6)$$

$$g - C_3N_4\left(e^-_{CB}\right) + H_2O_2 \rightarrow g - C_3N_4 + OH^- + OH^\bullet \quad (7)$$

In addition, g-C_3N_4 possesses high thermal stability (i.e., resistance to oxidation in air at a temperature of up to 600 °C) and is insoluble in water and organic solvents, contributing to the facile disinfection of viruses prevailing in wastewater and air. The unique biocompatible and non-toxic nature of g-C_3N_4 minimizes its interference during the virus inactivation process. These merits of g-C_3N_4 contribute to its pioneering performance in a wide range of applications, including wastewater treatment, microbial disinfection, environmental remediation, health care, and energy conversion. The dilemma of appropriately tailoring (lowering) the bandgap of g-C_3N_4 to promote the solar spectrum's utilization while simultaneously reducing the charge carrier recombination remains a significant drawback [55]. The other issues that could arise during the photocatalytic viral inactivation mechanism include: (i) the limited surface area of the g-C_3N_4 photocatalyst inhibiting ROS generation; (ii) agglomeration of g-C_3N_4 nanoparticles in water; (iii) controlled diffusion of surface-bound radicals; and (iv) the counterattack of released radicals with oxidizable substrates of the virus cell wall. As a solution, strategies such as heterojunction formation, doping, dye sensitization, and co-catalyst loading are introduced in bare g-C_3N_4 to increase the photoactivity [56,57]. To date, g-C_3N_4 has been well explored for bacterial disinfection via photocatalysis. In contrast, the photocatalytic disinfection of viruses is difficult to accomplish due to their vast range of classifications, varying composition, complex structure, and higher resistance to oxidative stress [58].

4. Antiviral Performance of Graphitic Carbon Nitride-Based Photocatalysts

To exploit the photocatalytic efficiency of g-C_3N_4 for virus inactivation under visible light irradiation, Li et al., for the first time, conducted an antiviral experiment using the bacteriophage MS2 as a model virus. As illustrated in Figure 2a, the major reactive oxidative species responsible for the 1×10^8 PFU/mL inactivation of bacteriophage MS2 were photogenerated electrons and $O_2^{\bullet-}$ radicals. The photocatalytic degradation mechanism

of MS2 involved oxidative damage to the surface protein, resulting in a shape distortion of the virus followed by disruption of the viral genome RNA, ultimately causing viral death with no regrowth for up to 72 h. The action of reactive oxidative species on the protein coating of the virus, which is shown in Figure 2b, was confirmed by the decrease in protein concentration from 9.8 mg/mL to 0 mg/mL for 1×10^8 PFU/mL of virus treated by 5 mL of g-C_3N_4 after 360 min of irradiation. A comparative study was performed to evaluate the efficacy of g-C_3N_4 compared with other photocatalysts, as shown in Figure 2c, which revealed more than 7-log, 1-log, and 4-log of MS2 deactivation by g-C_3N_4, N-doped TiO_2, and Bi_2WO_6, respectively. Ag@AgCl displayed higher inactivation of viruses of up to 8 log within 300 min, which was attributed to the biocidal and electron sink properties of Ag nanoparticles [28]. Because of the merits of Ag nanoparticles, a Ag_3PO_4/g-C_3N_4 Z-scheme heterojunction revealed the complete inactivation of the bacteriophage f2 virus by the action of released $OH^\bullet > h^+ > O_2^{\bullet -}$ radicals at a concentration of 3×10^6 PFU/mL within 80 min of irradiation. The photocatalytic inactivation efficiency had the following trend: g-C_3N_4, 3.6 log; Ag_3PO_4, 4.5 log; and Ag_3PO_4/g-C_3N_4, 6.5 log, which was attributed to the higher electron–hole pair separation and the more comprehensive visible light response (up to 500 nm) in Ag_3PO_4/g-C_3N_4. The higher photo-oxidative ability of Ag_3PO_4/g-C_3N_4 was evident from the photoluminescence spectra, which showed a 48% decrease in PL emission intensity compared with bare g-C_3N_4 [29].

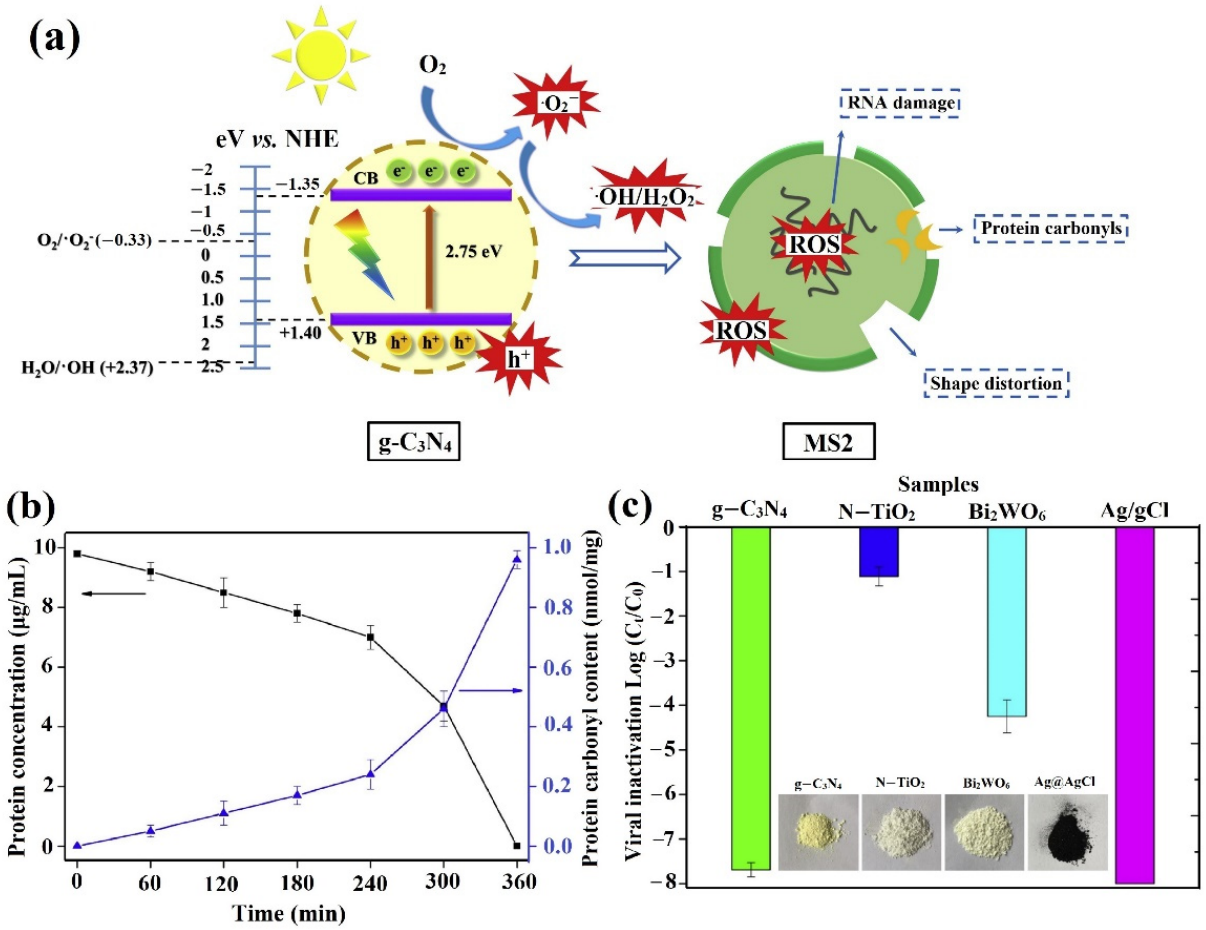

Figure 2. (**a**) Schematic representation of the viral inactivation mechanism of g-C_3N_4 under visible-light exposure; (**b**) protein concentration measurements in 100 μL of a solution of viral particle lysates from 5 mL of a virus-related suspension (1×10^8 PFU/mL) and the amount of protein carbonyls during the inactivation process; (**c**) photocatalytic activity of Ag@AgCl, Bi_2WO_6, N-TiO_2, and g-C_3N_4 samples with 150 mg/L dosages for MS2 inactivation upon exposure to visible light. Reproduced with permission from [28] with license number 5136360326508. Copyright Elsevier 2016.

The dual photoinactivation of an antibacterial (*E. coli*) and an antiviral (MS2) was investigated for the first time over a g-C_3N_4/expanded perlite 520 floating photocatalyst under visible light irradiation. The scavenging experiment showed that $OH^{\bullet}$ radicals were dominant in the MS2's inactivation, whereas $O_2^{\bullet-}$ radicals participated in both *E. coli* and MS2 inactivation. The different behavior of the photoinactivation mechanism was accredited to the different sizes and surface morphologies of *E. coli* bacteria and the MS2 virus. More importantly, the denaturation of the rigid capsid cell wall of the MS2 virus requires highly oxidizing $OH^{\bullet}$ radicals. The viral photocatalytic efficiency of the g-C_3N_4/expanded perlite 520 photocatalyst was practically assessed in deionized water and natural water, wherein a decrease in removal efficiency from 8 log to 3.7 log was obtained. This was attributed to the effect of natural organic matter constituents in natural water, which tend to absorb the floating g-C_3N_4/expanded perlite 520 photocatalyst, thereby blocking reactive oxidative species generation [30].

To further comprehend the photocatalytic viral inactivation mechanism in g-C_3N_4, Zhang et al. studied the effect of various operating parameters, including temperature and photocatalyst loading, within 180 min of visible light irradiation via 3D response surface and 2D contour plots. Figure 3a illustrates a variation in reaction temperature from 1.48 °C to 43.5 °C, where the maximum MS2 viral inactivation of 6.5 log PFU/mL was obtained at 24.05 °C compared with the g-C_3N_4 photocatalyst. The inhibition of viral inactivation at higher temperatures was due to the decrease in dissolved oxygen levels, which further lowered the concentration of $O_2^{\bullet-}$ radicals. Further, investigation of the effect of a photocatalyst loading from 15.91 to 135 mg /L resulted in an increase in MS2 inactivation efficiency due to the increased specific surface area of the g-C_3N_4 photocatalyst with a large number of active sites. The vital factor of light intensity required to induce electron–hole pair transitions was optimized at 199.80 mW/cm^2 concerning varying photocatalyst loadings (Figure 3b) and temperatures (Figure 3c) [27]. With the integrated merits of doping and the Z-scheme charge transfer mechanism, Zhang et al. evaluated the performance of O-doped g-C_3N_4 coupled with hydrothermal carbonation carbon on human adenovirus type 2. Figure 4a shows the virucidal mechanism, which depicts direct Z-scheme electron migration from the conduction band (−0.27 eV) of the hydrothermal carbonation carbon to the −0.86 eV conduction band of the O-doped g-C_3N_4. The enhanced electron–hole pair separation resulted in the generation of higher amounts of $O_2^{\bullet-}$ and $OH^{\bullet}$ radicals for the distortion and rupture of, and formation of holes in, human adenovirus type 2 viral capsids, as confirmed by TEM images, under 120 min of visible light irradiation, causing a loss of pathogenicity (Figure 4b). As shown in Figure 4c, the toxicity assessment of photocatalysts through an XTT proliferation colorimetric assay with human A549 lung carcinoma cells displayed negligible cell viability even at a higher concentration of 150 µg/mL of photocatalyst, indicating the excellent biocompatibility of the synthesized photocatalysts [31].

Based on the above-described literature, it is evident that the virucidal potential of g-C_3N_4-based photocatalysts has been well-explored for non-enveloped viruses.

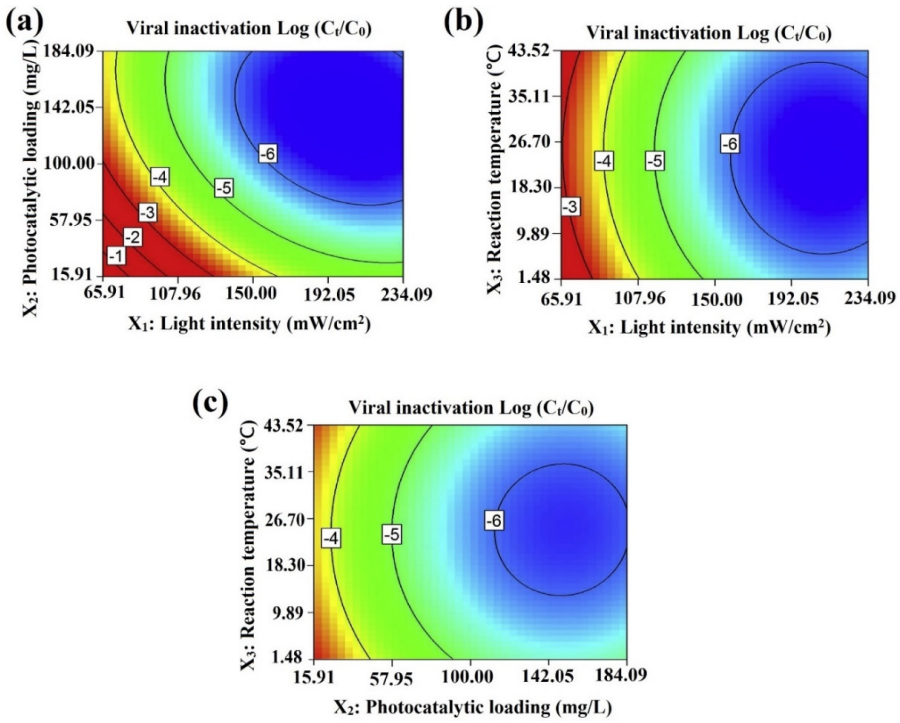

Figure 3. The plots demonstrate the photocatalytic viral inactivation efficacy by g-C_3N_4 of (**a**) photocatalytic loading X_2 vs. intensity of light X_1; (**b**) intensity of light X_1 vs. reaction temperature X_3; and (**c**) reaction temperature X_3 vs. photocatalytic loading X_2. Reproduced with permission from [27] with license number 5136341150728. Copyright Elsevier 2018.

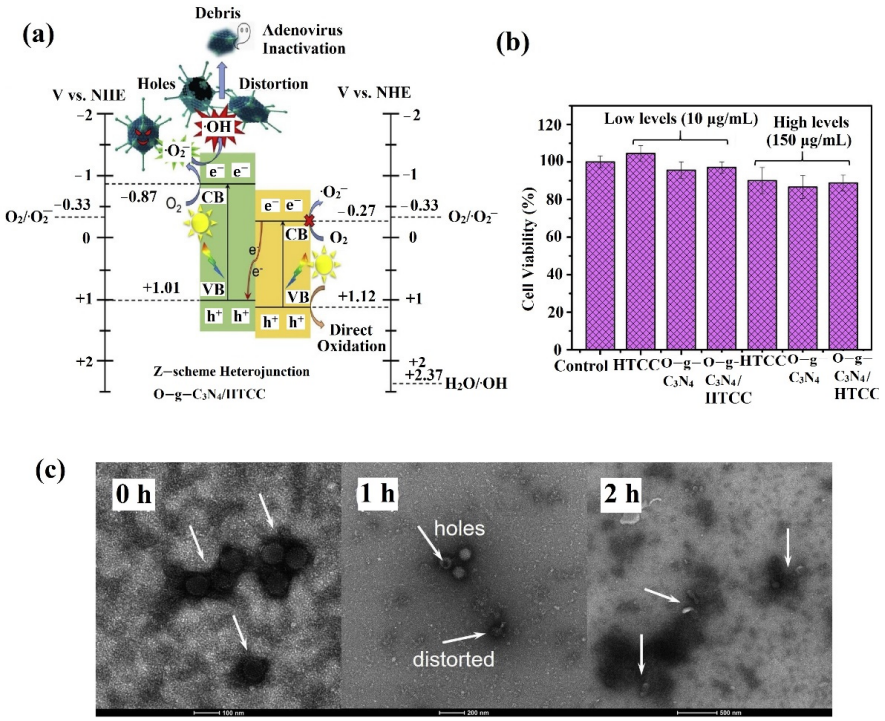

Figure 4. (**a**) The plausible charge transfer route in photocatalysis over the O-g-C_3N_4/HTCC Z-scheme heterojunction; (**b**) cytotoxic effects of O-g-C_3N_4/HTCC, and O-g-C_3N_4; and (**c**) TEM images of HAdV-2 mixed with O-g-C_3N_4/HTCC taken during different intervals of time. Reproduced with permission from [31] with license number 5136341407889. Copyright Elsevier 2021.

5. Promising Role of Graphitic Carbon Nitride-Based Photocatalysts in Healthcare

The development of modified g-C_3N_4-based photocatalysts with high water solubility and biodegradability, a small nanoscale size, and enhanced light absorption is important to the achievement of target-specific applications [59]. Various strategies and synthesis routes have been investigated in this respect. Subsequently, bare g-C_3N_4 and its derivatives were used in healthcare applications, particularly pathogenic biofilm control, diagnostic imaging, and therapeutics [60]. g-C_3N_4 possesses superior stability, good biocompatibility, low toxicity, a unique fluorescence emission, and high ROS production potential; hence, it may play a vital role in diagnosis and therapy. The following discussion summarizes the healthcare applications of graphitic carbon nitride-based photocatalysts based on ROS generated upon light irradiation.

- Pathogenic biofilm control: The issue of the unwanted growth of pathogenic biofilms on surfaces raises crucial health concerns since these bacteria can persist for a prolonged time. The most commonly contaminated surfaces are those of hospital equipment, packaging materials, and food-processing facilities, which can become vulnerable routes for disease transmission. The conventional disinfection strategies include UV-light irradiation, mechanical cleaning, and chemical sprays, which need to be frequently applied to maintain the efficacy of biofilm control. The photocatalysis process holds promise in biofilm control due to its broad-spectrum effectiveness under room conditions (ambient light/sunlight), simplicity, good recyclability, and low cost. For instance, the biofilm-dispersing ability of a Ag/g-C_3N_4 photocatalyst was assessed, wherein the attack of $O_2^{\bullet -}$ radicals resulted in complete degradation of the protein coating, exopolysaccharides, and nucleic acid of *S. aureus* biofilms [61]. The promising role of a g-C_3N_4/chitosan photocatalyst was revealed by the biofilm inhibition of *S. epidermidis*, *P. aeruginosa*, and *E. coli* in urine samples. The $^1O_2$ radicals released under visible light irradiation were dominant in the biofilms' eradication [62].
- Photodynamic therapy: The property of ROS generation under light illumination makes g-C_3N_4 a suitable candidate for destroying tumor cells by damaging the gene structure. Principally, the phenomena of photodynamic therapy involve the production of ROSs ($O_2^{\bullet -}$ and $OH^{\bullet}$ radicals), which block the electron transport chain in mitochondria, resulting in a lack of supply of energy and nutrients to tumor cells, leading to cell death. The photosensitization effect of Ru coordinated to g-C_3N_4 has been exploited for the photodynamic therapy of hypoxic tumor cells as explained in the mechanism shown in Figure 5a. The invasion of hypoxic tumor cells by Ru^{+2}-g-C_3N_4 occurs under visible light irradiation involving photoinduced reduction of the Ru^{+3} center to the Ru^{+2} center to generate multiple cytotoxic ROSs ($OH^{\bullet}$, $O_2^{\bullet -}$, and $^1O_2$), which causes mitochondrial dysfunction leading to apoptosis [63].
- Wound healing: The ROSs generated under light irradiation tend to inhibit the growth of bacteria and act as wound healers. The accelerated wound healing performance was evaluated for a Z-scheme ZnO/C-dots/g-C_3N_4 ternary heterojunction (Figure 5b), wherein C-dots serve as a bridge to reduce electron–hole pair recombination for the migration of electrons from the conduction band of ZnO to the valence band of g-C_3N_4. The subsequent production of $OH^{\bullet}$ and $^1O_2$ radicals resulted in 99.97% and 99.8% disinfection of *Streptococcus aureus* and *Escherichia coli*, respectively. The released Zn^{+2} intruded into the bacteria and exhibited a hyperthermia effect, triggering the growth of fibroblasts for a rapid wound healing process [64].
- Bioimaging: The quantum confinement and edge effects of g-C_3N_4 photocatalysts limit the electron mobility, contributing to fluorescence emissions. In addition, g-C_3N_4 emits wavelengths of blue and green light that can be optically tuned to enhance the fluorescence quantum efficiency for cell imaging to display a contrasting image. Zhang et al. performed neuronal differentiation of PC12 cells using the phenomena of non-invasive light stimulation. Under visible light irradiation (450 nm), the biocompatible interface of g-C_3N_4/graphene photocatalysts dispersed on polycaprolactone/gelatin fibers

exhibited distinguished outgrowth of neurite while simultaneously improving the electron–hole pair charge carrier separation as demonstrated in Figure 5c [65].

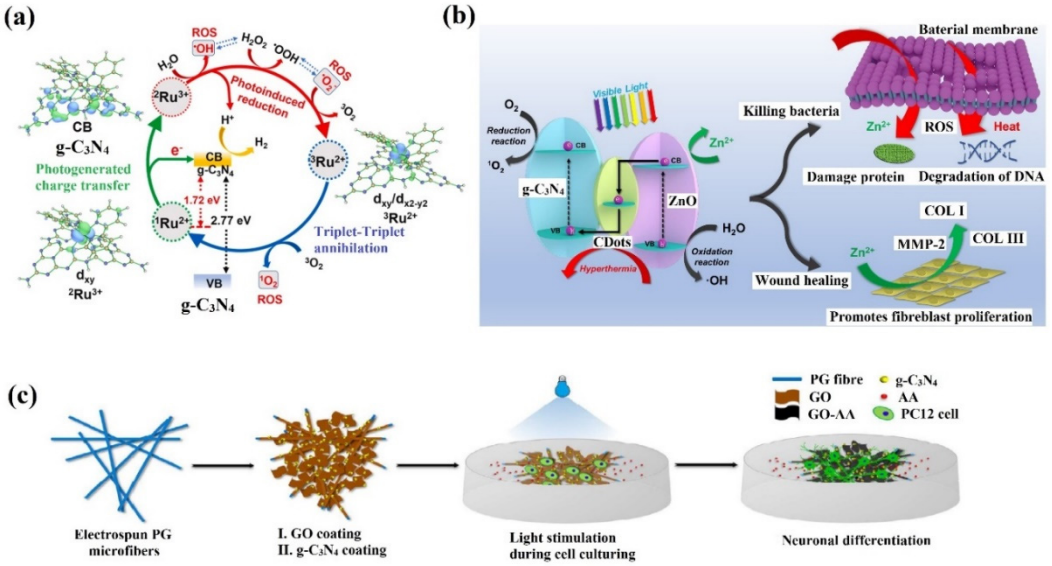

Figure 5. (**a**) The photocatalytic $^1O_2$ generation mechanism of Ru-g-C_3N_4 in the presence of H_2O_2 or H_2O. The superscripts on the Ru ions denote the ground state Ru^{2+}, the triplet state Ru^{2+}, and the radical, cationic species Ru^{3+}; (**b**) schematic representation of ZnO/CDots/g-C_3N_4 Z-schemes for photo-assisted bacteria inactivation; (**c**) diagrammatic illustration of the growth of neural PC12 cells on g-C_3N_4/graphene composite fibers on exposure to visible light. Reproduced with permission from [63–65] with license numbers 5161471258951 and 5161480119676. Copyright American Chemical Society 2017, Elsevier 2020, 2021.

6. Challenges and Sustainable Solutions

Despite the performance of g-C_3N_4-based photocatalysts in diverse applications, the research, perception, and interpretation remain in their infancy with respect to the virus inactivation mechanism and large-scale practical efficiency. In the race to fully explore and utilize g-C_3N_4-based photocatalysts for virus disinfection purposes, we need to put in effort to identify possible solutions to overcome the prevailing challenges. In this respect, it can be roughly divided into the following aspects:

- Insufficient validation of the reaction mechanism: our understanding of the characterization techniques for validating the photocatalytic virus disinfection mechanism is insufficient to support: (i) the extent of ROS generation; (ii) the co-existing action of $O_2^{\bullet -}$ and $OH^{\bullet}$ radicals in attacking the virus cell wall; (iii) the pathway selectivity during viral mutation; and (iv) the offensive response of the virus upon exposure to light irradiation. Another significant challenge involves the stronger resistance of certain viruses to UVC (200–280 nm), UVB (280–320 nm), and UVA (320–400 nm) light, which requires the development of visible-light-active or near-infrared-responsive photocatalysts [66]. It is thus necessary to precisely identify and characterize the role of participating ROSs to obtain a reasonable photocatalytic virus disinfection mechanism for the amendment of a practical photocatalysis process.
- Photostability, recyclability, and scalable production are the most crucial factors in the enhancement of the efficacy and robustness of g-C_3N_4-based photocatalysts that target virus eradication [67]. Considering the extended time during which viruses persist in the environment (air, water, and infected surfaces), the stability of g-C_3N_4 photocatalysts needs to be enhanced to overcome the economic barriers. The improvement of the current separation techniques for recovery of g-C_3N_4 photocatalysts from wastewater and photoreactors is recommended to solve the challenging issue of photocatalysts' recyclability [68]. In accordance, magnetic isolation via the incorporation of nanosized suspended particles into the contaminated reaction mixture has been explored [69]. In

terms of the large-scale production and applicability of g-C_3N_4 photocatalysts, cost-effective engineering strategies should be practiced, and photoreactor designs need to be optimized for extended solar energy utilization. Hence, the commercialization of metal-free g-C_3N_4 material is vital at the industrial scale for the future mass utilization of solar energy with a minimal environmental impact. The photoreactor design needs to be optimized for an increased light-capturing rate with the maximum use of renewable sunlight to achieve the sustainable disinfection of viruses. The most suitable photoreactor is the compound parabolic collector (CPC), which effectively utilizes diffuse and direct solar irradiation. Hence, the commercialization of photoreactors is vital at the industrial scale for the future mass utilization of solar energy with a minimal environmental impact [42].

- Conflicting band edge modulation achieves broad-spectrum solar energy absorption while maintaining a high redox potential with a reduced electron–hole pair recombination rate. The type II and Z-scheme charge transfer routes are two cutting-edge strategies for solving these predicaments [70,71]. Based on our critical assessment, it is not surprising that g-C_3N_4-based photocatalysts have benefitted a diverse range of photocatalytic fields. As a matter of course, it is expected that the above challenges will be resolved with advances in research. Even though various disinfection technologies have been developed to mitigate the spread of viruses, photocatalytic virus disinfection is a sustainable alternative that may lessen the environmental impact.

7. Conclusions

This article provides an overview of virus disinfection by the semiconductor photocatalysis process to address the problems associated with virus pandemics. The unique merits of g-C_3N_4-based photocatalysts and their utilization in diverse fields, including energy, environment, and biomedicine-related applications, have instigated researchers to provide perspectives on g-C_3N_4-driven virus disinfection. Their development is emerging and rapidly progressing owing to their metal-free, visible-light-active, non-toxic, and biocompatible nature for the next generation of sustainable virus eradication techniques. It was discovered that the critical photocatalytic virus inactivation mechanism for g-C_3N_4 involves the action of reactive oxidative species (ROSs), mainly $O_2^{\bullet -}$ and $OH^{\bullet}$ radicals, which rupture the capsid shell, deactivate proteins, damage genes, and eventually inhibit virus regrowth. This article reviewed and assessed the latest advancements in g-C_3N_4-based photocatalysts for virus inactivation. The photocatalysis operating parameters, such as temperature, light intensity, photocatalyst concentration, pH, and the effect of organic matter, affecting the antiviral performance of g-C_3N_4 have been well-explored to enhance the reactive oxidative species production rate and maximize the visible light spectrum's utilization. The contributions of g-C_3N_4-based photocatalysts in healthcare applications, including bioimaging, therapeutics, and bacterial biofilm control, exemplify the prominent role of the ROSs released under visible light irradiation. However, particular long-term challenges remain regarding both g-C_3N_4 and the photocatalysis process, which restrict the large-scale applicability of g-C_3N_4-based photocatalysts in virus disinfection. Future studies should undertake pilot-scale photoreactor research and fill the remaining knowledge gaps on the exact photocatalytic viral inactivation mechanism. We hope that this review helps to realize the potential of photocatalysis as an alternative sustainable technology to prevent the regrowth of viruses.

Author Contributions: V.H.: Writing—original draft preparation-review and editing, methodology; S.P.: Writing-review and editing, methodology; P.S.: supervision, project administration, writing—review and editing; V.-H.N.: supervision, writing—review and editing; Q.V.L.: conceptualization, methodology; V.K.T.: conceptualization, methodology; C.M.H.: conceptualization, methodology; R.S.: conceptualization, methodology; C.-W.H.: funding acquisition, writing—review and editing; S.T.: conceptualization, methodology; P.R.: conceptualization, supervision, writing—review and editing. All authors have read and agreed to the published version of the manuscript.

Funding: This research was funded by the Ministry of Science and Technology (MOST) in Taiwan, grant number MOST 110-2221-E-992 -030-MY3.

Conflicts of Interest: The authors declare no conflict of interest.

References

1. Perkins, K.M.; Munguia, N.; Ellenbecker, M.; Eraso, R.M.; Velazquez, L. COVID-19 pandemic lessons to facilitate future engagement in the global climate crisis. *J. Clean. Prod.* **2021**, *290*, 125178. [CrossRef]
2. Covid, W. Coronavirus Pandemic. Available online: https://www.worldometers.info/coronavirus (accessed on 28 July 2021).
3. Lewis, D. Is the coronavirus airborne? Experts can't agree. *Nature* **2020**, *580*, 175. [CrossRef]
4. Kumar, A.; Singh, P.; Raizada, P.; Hussain, C.M. Impact of COVID-19 on greenhouse gases emissions: A critical review. *Sci. Total Environ.* **2022**, *860*, 150349. [CrossRef] [PubMed]
5. World Health Organization. *WHO Coronavirus (COVID-19) Dashboard*; World Health Organization: Geneva, Switzerland, 2021. Available online: https://covid19.who.int/ (accessed on 10 June 2021).
6. Srivastava, A.K.; Dwivedi, N.; Dhand, C.; Khan, R.; Sathish, N.; Gupta, M.K.; Kumar, R.; Kumar, S. Potential of graphene-based materials to combat COVID-19: Properties, perspectives and prospects. *J. Mater. Today Chem.* **2020**, *18*, 100385. [CrossRef]
7. Seifi, T.; Kamali, A.R. Antiviral performance of graphene-based materials with emphasis on COVID-19: A review. *Int. J. Drug Discov.* **2021**, *11*, 100099. [CrossRef]
8. Innocenzi, P.; Stagi, L. Carbon-based antiviral nanomaterials: Graphene, C-dots, and fullerenes. A perspective. *Chem. Sci.* **2020**, *11*, 6606–6622. [CrossRef] [PubMed]
9. Tseng, C.; Li, C. Inactivation of surface viruses by gaseous ozone. *J. Environ. Health* **2008**, *70*, 56–63.
10. Hasija, V.; Nguyen, V.H.; Kumar, A.; Raizada, P.; Krishnan, V.K.; Khan, A.A.P.; Singh, P.; Lichtfouse, E.; Wang, C.; Huong, P.T. Advanced activation of persulfate by polymeric g-C_3N_4 based photocatalysts for environmental remediation: A review. *J. Hazard. Mater.* **2021**, *413*, 125324. [CrossRef] [PubMed]
11. Nandan, A.; Siddiqui, N.A.; Singh, C.; Aeri, A.; Gwenzi, W.; Ighalo, J.O.; Nagliate, P.; Singh, P. COVID-19 pandemic in Uttarakhand, India: Environmental recovery or degradation? *J. Environ. Chem. Eng.* **2021**, *9*, 106595. [CrossRef]
12. Mahmoudian, L.; Jashni, A.K.; Hosseini, S.N.; Paryan, M. Optimization of rDNA degradation in recombinant Hepatitis B vaccine production plant wastewater using visible light excited Ag-doped TiO_2 nano-photocatalyst. *Process Saf. Environ. Prot.* **2019**, *122*, 328–338. [CrossRef]
13. Zan, L.; Fa, W.; Peng, T.; Gong, Z.K. Photocatalysis effect of nanometer TiO_2 and TiO_2-coated ceramic plate on Hepatitis B virus. *J. Photochem. Photobiol.* **2007**, *86*, 165–169. [CrossRef] [PubMed]
14. Guo, B.; Snow, S.D.; Starr, B.J.; Xagoraraki, I.; Tarabara, V.V. Photocatalytic inactivation of human adenovirus 40: Effect of dissolved organic matter and prefiltration. *Sep. Purif. Technol.* **2018**, *193*, 193–201. [CrossRef]
15. Hajkova, P.; Spatenka, P.P.; Horsky, J.; Horska, I.; Kolouch, A. Photocatalytic effect of TiO_2 films on viruses and bacteria. *Plasma Process Polym.* **2007**, *4*, S397–S401. [CrossRef]
16. Cui, H.; Jiang, J.; Gu, W.; Sun, C.; Donglai, W.; Yang, T.; Yang, G. Photocatalytic Inactivation Efficiency of Anatase Nano-TiO_2 Sol on the H9N2 Avian Influenza Virus. *Photochem. Photobiol.* **2010**, *86*, 1135–1139. [CrossRef]
17. Nakano, R.; Ishiguro, H.; Yao, Y.; Kajioka, J.; Fujishima, A.; Sunada, K.; Minoshima, M.; Hashimoto, K.; Kubota, Y. Photocatalytic inactivation of influenza virus by titanium dioxide thin film. Photochem. *Photobiol. Sci.* **2012**, *11*, 1293–1298. [CrossRef]
18. Park, D.; Shahbaz, H.M.; Kim, S.H.; Lee, M.; Lee, W.; Oh, J.W.; Lee, D.U.; Park, J. Inactivation efficiency and mechanism of UV-TiO_2 photocatalysis against murine norovirus using a solidified agar matrix. *Int. J. Food Microbiol.* **2016**, *238*, 256–264. [CrossRef]
19. Moon, W.E.; Hae, L.W.; Jeong, R.H.; Ji, H.H. Photocatalytic inactivation of viral particles of human norovirus by Cu-doped TiO_2 non-woven fabric under UVA-LED wavelengths. *Sci. Total Environ.* **2020**, *749*, 141574. [CrossRef]
20. Jeong, K.M.; Lee, J.E.; Seok, K.S.; Kim, K.H.; Seung, M.C.; Lee, G. Effects of Calcination Temperature on the Phase Composition, Photocatalytic Degradation, and Virucidal Activities of TiO_2 Nanoparticles. *ACS Omega* **2021**, *6*, 10668–10678.
21. Mahon, M.; Joanne, S.C.; Kelly, P.J.M.; Gill, L.W. Solar photocatalytic disinfection of E. coli and bacteriophages MS2, ΦX174 and PR772 using TiO_2, ZnO and ruthenium-based complexes in a continuous flow system. *J. Photochem. Photobiol.* **2017**, *170*, 79–90. [CrossRef]
22. Hu, X.; Hu, C.; Peng, T.; Zhou, X.; Qu, J. Plasmon-induced inactivation of enteric pathogenic microorganisms with Ag-AgI/Al_2O_3 under visible-light irradiation. *Enviro. Sci. Technol.* **2010**, *44*, 7058–7062. [CrossRef]
23. Takehara, K.; Yamazaki, K.; Miyazaki, M.; Yamada, Y.; Ruenphet, S.; Jahangir, A.; Shoham, D.; Okamura, M.; Nakamura, M. Inactivation of avian influenza virus H1N1 by photocatalyst under visible light irradiation. *Virus Res.* **2010**, *151*, 102–103. [CrossRef]
24. Käsermann, F.; Kempf, C. Photodynamic inactivation of enveloped viruses by buckminsterfullerene. *Antivir. Res.* **1997**, *34*, 65–70. [CrossRef]
25. Moor, K.J.; Kim, J.H. Simple synthetic method toward solid supported C60 visible light-activated photocatalysts. *Environ. Sci. Technol.* **2014**, *48*, 2785–2791. [CrossRef] [PubMed]
26. Moor, K.J.; Valle, D.C.; Li, C.; Kim, J.-H. Improving the visible light photoactivity of supported fullerene photocatalysts through the use of [C70] fullerene. *Environ. Sci. Technol.* **2015**, *49*, 6190–6197. [CrossRef]

27. Zhang, C.; Li, Y.; Zhang, W.; Wang, P.; Wang, C. Metal-free virucidal effects induced by g-C_3N_4 under visible light irradiation: Statistical analysis and parameter optimization. *Chemosphere* **2018**, *195*, 551–558. [CrossRef] [PubMed]
28. Li, Y.; Zhang, C.; Shuai, D.; Naraginti, S.; Wang, D.; Zhang, W. Visible-light-driven photocatalytic inactivation of MS2 by metal-free g-C_3N_4: Virucidal performance and mechanism. *Water Res.* **2016**, *106*, 249–258. [CrossRef]
29. Cheng, R.; Liang, S.J.; Yu, J.H.; Shao, X. Photocatalytic inactivation of bacteriophage f2 with Ag_3PO_4/g-C_3N_4 composite under visible light irradiation: Performance and mechanism. *Catalysts* **2018**, *8*, 406. [CrossRef]
30. Zhang, C.; Li, Y.; Danmeng, S.; Wenlong, Z.; Lihua, N.; Longfe, W.; Huanjun, Z. Visible-light-driven, water-surface-floating antimicrobials developed from graphitic carbon nitride and expanded perlite for water disinfection. *Chemosphere* **2018**, *208*, 84–92. [CrossRef]
31. Zhang, C.; Mengyang, Z.; Yi, L.; Danmeng, S. Visible-light-driven photocatalytic disinfection of human adenovirus by a novel heterostructure of oxygen-doped graphitic carbon nitride and hydrothermal carbonation carbon. *Appl. Catal. B Environ.* **2019**, *248*, 11–21. [CrossRef]
32. Kessler, F.K.; Zheng, Y.; Schwarz, D.; Merschjann, C.; Schnick, W.; Wang, X.; Bojdys, M.J. Functional carbon nitride materials—design strategies for electrochemical devices. *Nat. Rev. Mater.* **2017**, *2*, 17030. [CrossRef]
33. Liu, J.; Wang, H.; Antonietti, H.M. Graphitic carbon nitride "reloaded": Emerging applications beyond (photo) catalysis. *Chem. Soc. Rev.* **2016**, *45*, 2308–2326. [CrossRef] [PubMed]
34. Hasija, V.; Raizada, P.; Sudhaik, A.; Singh, P.; Thakur, V.K.; Khan, A.A.P. Fabrication of Ag/AgI/WO_3 heterojunction anchored P and S co-doped graphitic carbon nitride as a dual Z scheme photocatalyst for efficient dye degradation. *J. Solid State Sci.* **2020**, *100*, 106095. [CrossRef]
35. Raizada, P.; Nguyen, V.H.; Patial, S.; Singh, P.; Bajpai, A.; Khan, A.A.P.; Rangabhashiyam, S. Toward practical solar-driven photocatalytic water splitting on two-dimensional MoS_2 based solid-state Z-scheme and S-scheme heterostructure. *Fuel* **2021**, *303*, 121302. [CrossRef]
36. Hasija, V.; Raizada, P.; Singh, P.; Verma, N.; Khan, A.A.P.; Singh, A.; Selvasembian, R. Progress on the photocatalytic reduction of hexavalent Cr (VI) using engineered graphitic carbon nitride. *Process Saf. Environ. Prot.* **2021**, *152*, 663–678. [CrossRef]
37. Mallakpour, S.; Azadi, E.; Hussain, C.M. The latest strategies in the fight against the COVID-19 pandemic: The role of metal and metal oxide nanoparticles. *New J. Chem.* **2021**, *45*, 6167–6179. [CrossRef]
38. Soni, V.; Raizada, P.; Kumar, A.; Hasija, V.; Singal, S.; Singh, P.; Bandegharaei, A.H.; Thakur, V.K.; Huy, V.H. Indium sulfide-based photocatalysts for hydrogen production and water cleaning: A review. *Environ. Chem. Lett.* **2021**, *19*, 1065–1095. [CrossRef]
39. Mallakpour, S.; Elham, A.; Chaudhery, M.H. Fight against COVID-19 pandemic with the help of carbon-based nanomaterials. *New J. Chem.* **2021**, *45*, 8832–8846. [CrossRef]
40. Sjogren, J.C.; Sierka, R.A. Inactivation of phage MS2 by iron-aided titanium dioxide photocatalysis. *Appl. Environ. Microbiol.* **1994**, *60*, 344–347. [CrossRef]
41. Upadhyay, R.K.; Soin, N.; Roy, S.S. Role of graphene/metal oxide composites as photocatalysts, adsorbents and disinfectants in water treatment: A review. *RSC Adv.* **2014**, *4*, 3823–3851. [CrossRef]
42. Cho, M.; Lee, J.; Mackeyev, Y.; Wilson, L.J.; Alvarez, P.J.; Hughes, J.B.; Kim, J.-H. Visible light sensitized inactivation of MS-2 bacteriophage by a cationic amine-functionalized C60 derivative. *Environ. Sci. Technol.* **2010**, *44*, 6685–6691. [CrossRef]
43. Zhang, C.; Li, Y.; Shuai, D.; Shen, Y.; Wang, D. Progress and challenges in photocatalytic disinfection of waterborne viruses: A review to fill current knowledge gaps. *Chem. Eng. J.* **2019**, *355*, 399–415. [CrossRef]
44. Raizada, P.; Hasija, V.; Singh, P.; Thakur, V.K. Carbon Nitride/Metal Oxide Hybrids for Visible Light Harvesting and Water Remediation. In *Water Pollution and Remediation: Photocatalysis*; Environmental Chemistry for a Sustainable World, Springer: Berlin, Germany, 2021; Volume 57, pp. 53–79.
45. Hasija, V.; Raizada, P.; Thakur, V.K.; Khan, A.A.P.; Asiri, A.M.; Singh, P. An overview of strategies for enhancement in photocatalytic oxidative ability of MoS_2 for water purification. *J. Environ. Chem. Eng.* **2020**, *8*, 104307. [CrossRef]
46. Nasir, A.M.; Awang, N.; Hubadillah, S.K.; Jaafar, J.; Othman, M.H.D.; Salleh, W.N.W.; Ismail, A.F. A review on the potential of photocatalysis in combatting SARS-CoV-2 in wastewater. *J. Water Process Eng.* **2021**, *42*, 102111. [CrossRef]
47. Wigginton, K.R.; Tamar, K. Virus disinfection mechanisms: The role of virus composition, structure, and function. *Curr. Opin. Virol.* **2012**, *2*, 84–89. [CrossRef] [PubMed]
48. Costa, L.; Faustino, M.A.F.; Neves, M.G.P.; Cunha, Â.; Almeida, A. Photodynamic inactivation of mammalian viruses and bacteriophages. *Viruses* **2012**, *4*, 1034–1074. [CrossRef]
49. Korneev, D.; Kurskaya, O.; Sharshov, K.; Eastwood, J.; Strakhovskaya, M. Ultrastructural aspects of photodynamic inactivation of highly pathogenic avian H5N8 influenza virus. *Viruses* **2019**, *11*, 955. [CrossRef] [PubMed]
50. Kumar, A.; Raizada, P.; Bandegharaei, A.H.; Thakur, V.K.; Nguyen, V.H.; Singh, P. C-, N-Vacancy defect engineered polymeric carbon nitride towards photocatalysis: Viewpoints and challenges. *J. Mater. Chem. A* **2021**, *9*, 111–153. [CrossRef]
51. Raizada, P.; Kumar, A.; Singh, P. Graphitic carbon nitride-based new advanced materials for photocatalytic applications. *J. Curr. Anal. Chem.* **2020**, *16*, 1-00. [CrossRef]
52. Zhang, C.; Li, Y.; Shuai, D.; Shen, Y.; Xiong, W.; Wang, L. Graphitic carbon nitride (g-C_3N_4)-based photocatalysts for water disinfection and microbial control: A review. *Chemosphere* **2019**, *214*, 462–479. [CrossRef]
53. Xu, J.; Wang, Z.; Zhu, Y. Enhanced visible-light-driven photocatalytic disinfection performance and organic pollutant degradation activity of porous g-C_3N_4 nanosheets. *Appl. Mater. Interfaces* **2017**, *9*, 27727–27735. [CrossRef]

54. Hasija, V.; Patial, S.; Raizada, P.; Khan, A.A.P.; Asiri, A.M.; Nguyen, Q.V.L.V.H.; Singh, P. Covalent organic frameworks promoted single metal atom catalysis: Strategies and applications. *Coord. Chem. Rev.* **2022**, *452*, 214298. [CrossRef]
55. Murugesan, P.; Moses, J.; Anandharamakrishnan, C. Photocatalytic disinfection efficiency of 2D structure graphitic carbon nitride-based nanocomposites: A review. *J. Mater. Sci.* **2019**, *54*, 12206–12235. [CrossRef]
56. Kumar, A.; Hasija, V.; Sudhaik, A.; Raizada, P.; Quyet, V.L.; Singh, P.; Pham, T.H.; Young, T.Y.; Ghotekar, S.; Nguyen, V.H. Artificial leaf for light-driven CO_2 reduction: Basic concepts, advanced structures and selective solar-to-chemical products. *Chem. Eng. J.* **2021**, *430*, 133031. [CrossRef]
57. Hasija, V.; Kumar, A.; Sudhaik, A.; Raizada, P.; Singh, P.; Quyet, V.L.; Le, T.T.; Nguyen, V.H. Step-scheme heterojunction photocatalysts for solar energy, water splitting, CO_2 conversion, and bacterial inactivation: A review. *Environ. Chem. Lett.* **2021**, *19*, 2941–2966. [CrossRef]
58. Raizada, P.; Kumar, A.; Hasija, V.; Singh, P.; Thakur, V.K.; Khan, A.A.P. An overview of converting reductive photocatalyst into all solid-state and direct Z-scheme system for water splitting and CO_2 reduction. *J. Ind. Eng. Chem.* **2021**, *93*, 1–27. [CrossRef]
59. Khan, A.A.P.; Singh, P.; Raizada, P.; Asiri, A.M. Converting Ag_3PO_4/CdS/Fe doped C_3N_4 based dual Z-scheme photocatalyst into photo-Fenton system for efficient photocatalytic phenol removal. *J. Ind. Eng. Chem.* **2021**, *98*, 148–160. [CrossRef]
60. Chan, M.H.; Liu, R.S.; Hsiao, M. Graphitic carbon nitride-based nanocomposites and their biological applications: A review. *Nanoscale* **2019**, *11*, 14993–15003. [CrossRef] [PubMed]
61. Zhou, Z.; Zhang, Y.; Shen, Y.; Liu, S.; Zhang, Y. Molecular engineering of polymeric carbon nitride: Advancing applications from photocatalysis to biosensing and more. *Chem. Soc. Rev.* **2018**, *47*, 2298–2321. [CrossRef]
62. Bing, W.; Chen, Z.; Sun, H.; Shi, P.; Gao, N.; Ren, J.; Qu, X. Visible-light-driven enhanced antibacterial and biofilm elimination activity of graphitic carbon nitride by embedded Ag nanoparticles. *Nano Res.* **2015**, *8*, 1648–1658. [CrossRef]
63. Shen, H.; Durkin, D.P.; Aiello, A.; Diba, T.; Lafleur, J.; Zara, J.M.; Shen, Y.; Shuai, D. Photocatalytic graphitic carbon nitride-chitosan composites for pathogenic biofilm control under visible light irradiation. *J. Hazard. Mater.* **2021**, *408*, 124890. [CrossRef]
64. Wei, F.; Kuang, S.; Rees, T.W.; Liao, X.; Liu, J.; Luo, D.; Wang, J.; Zhang, X.; Ji, L.; Chao, H. Ruthenium (II) complexes coordinated to graphitic carbon nitride: Oxygen self-sufficient photosensitizers which produce multiple ROS for photodynamic therapy in hypoxia. *Biomaterials* **2021**, *276*, 121064. [CrossRef]
65. Xiang, Y.; Zhou, Q.; Li, Z.; Cui, Z.; Liu, X.; Liang, Y.; Zhu, S.; Zheng, Y.; Yeung, K.W.; Wu, S. A Z-scheme heterojunction of ZnO/CDots/C_3N_4 for strengthened photoresponsive bacteria-killing and acceleration of wound healing. *J. Mater. Sci.* **2020**, *57*, 1–11. [CrossRef]
66. Zhang, Z.; Xu, R.; Wang, Z.; Dong, M.; Cui, B.; Chen, M. Visible-light neural stimulation on graphitic-carbon nitride/graphene photocatalytic fibers. *Appl. Mater. Interfaces* **2017**, *9*, 34736–34743. [CrossRef]
67. Wang, W.; Zhou, C.; Yang, Y.; Zeng, G.; Zhang, C.; Zhou, Y.; Yang, J.; Huang, D.; Wang, H.; Xiong, W. Carbon nitride based photocatalysts for solar photocatalytic disinfection, can we go further? *J. Chem. Eng. J.* **2021**, *404*, 126540. [CrossRef]
68. Wang, L.; Wang, K.; He, T.; Zhao, Y.; Song, H.; Wang, H. Graphitic Carbon Nitride-Based Photocatalytic Materials: Preparation Strategy and Application. *Sustain. Chem. Eng.* **2020**, *8*, 16048–16085. [CrossRef]
69. Jia, C.; Yang, L.; Zhang, Y.; Zhang, X.; Xiao, K.; Xu, J.; Liu, J. Graphitic carbon nitride films: Emerging paradigm for versatile applications. *Appl. Mater. Interfaces* **2020**, *12*, 53571–53591. [CrossRef] [PubMed]
70. Sudhaik, A.; Raizada, P.; Shandilya, P.; Singh, P. Magnetically recoverable graphitic carbon nitride and $NiFe_2O_4$ based magnetic photocatalyst for degradation of oxytetracycline antibiotic in simulated wastewater under solar light. *J. Environ. Chem. Eng.* **2018**, *6*, 3874–3883. [CrossRef]
71. He, D.; Zhang, Z.; Xing, Y.; Zhou, Y.; Yang, H.; Liu, H.; Qu, J.; Yuan, X.; Guan, J.; Zhang, Y. Black phosphorus/graphitic carbon nitride: A metal-free photocatalyst for "green" photocatalytic bacterial inactivation under visible light. *Chem. Eng. J.* **2020**, *384*, 123258. [CrossRef]